Electronic Supplementary Material (ESI) for Chemical Science.
This journal is © The Royal Society of Chemistry 2022

Electronic Supplementary Information for:

Origin of intersystem crossing in highly distorted organic molecules: a case study with red light-absorbing *N,N,O,O*–boron–chelated Bodipys

Xue Zhang,‡[a] Andrey A. Sukhanov,‡[b] Xi Liu,‡[c] Maria Taddei,[d] Jianzhang Zhao,*[a] Anthony Harriman,*[e] Violeta K. Voronkova,*[b] Yan Wan,*[c] Bernhard Dick*[f] and Mariangela Di Donato*[d,g]

[a] State Key Laboratory of Fine Chemicals, Frontiers Science Center for Smart Materials, School of Chemical Engineering, Dalian University of Technology, Dalian 116024, P. R. China.
*E-mail: zhaojzh@dlut.edu.cn (J. Z.)

[b] Zavoisky Physical-Technical Institute, FRC Kazan Scientific Center of Russian Academy of Sciences, Kazan 420029, Russia. *E-mail: vio@kfti.knc.ru (V. K. V.)

[c] College of Chemistry, Beijing Normal University, Beijing 100875 P. R. China
*E-mail: wanyan@bnu.edu.cn (Y. W.)

[d] LENS (European Laboratory for Non-Linear spectroscopy), Via N. Carrara 1, 50019 Sesto Fiorentino (FI), Italy.
*E-mail: didonato@lens.unifi.it (M. D. D.)

[e] The Molecular Photonics Laboratory, School of Natural Sciences, University of Newcastle, Newcastle upon Tyne, NE1 7RU, United Kingdom.
*E-mail: anthony.harriman@newcastle.ac.uk (A.H.)

[f] Lehrstuhl für Physikalische Chemie, Institut für Physikalische und Theoretische Chemie, Universität Regensburg, D-93053 Regensburg, Germany.
*E-mail: Bernhard.Dick@chemie.uni-regensburg.de (B. D.)

[g] ICCOM, Istituto di Chimica dei Complessi OrganoMetallici, Via Madonna del Piano 10, 50019, Sesto Fiorentino (FI), Italy.

‡ These authors contributed equally to this work.

Contents

1. General Information and Synthesis

All the chemicals used in synthesis are analytically pure and were used as received, the solvents were dried and distilled before synthesis. ^{1}H and ^{13}C NMR spectra were recorded on the Bruker Avance spectrometers (400 MHz or 600 MHz). The mass spectra were measured by MALDI–TOF–HRMS spectrometer.

The synthesis of the compounds were according to the following steps:

1.1. Compound Mp-py (2-(2-Methoxyphenyl)-1H-pyrrole). NaH (800 mg, 20.0 mmol, 60% in mineral oil, 4.0 eq) was added in a 100 ml two-necked bottle, dry tetrahydrofuran (THF) (4 mL) as solvent was added slowly to obtain a suspension. Pyrrole (1.34 g, 1.38 mL, 20.0 mmol, 4.0 eq) was then carefully added. The resulting mixture was stirred until no further gas was formed. At this point, a solution of anhydrous $ZnCl_2$ (2.7 g dissolved in 16 ml of dry THF, 20 mmol, 4.0 eq) was slowly added (a exothermic process) and the mixture was stirred for 30 minutes. 2-Chloro methoxy benzene (713 mg, 5.0 mmol, 1.0 eq) was then added followed by JohnPhos (7.44 mg, 0.025 mmol, 0.005 eq) and palladium (II) acetate (5.61 mg, 0.025 mmol, 0.005 eq). The mixture was heated under reflux for 24 hours. After the reaction was completed, it was quenched with water and extracted with dichloromethane (DCM). The organic layer was separated and washed with water and brine solution, respectively. The organic layer was dried over anhydrous Na_2SO_4 and the solvent was evaporated under reduced pressure. The crude product was washed with *n*-hexane (HEX) and recrystallized in ether to give pure product as pale yellow solid (425 mg, yield: 49%). ^{1}H NMR (400 MHz, $CDCl_3$): δ = 9.83 (s, 1H), 7.68–7.65 (m, 1H), 7.18–7.14 (m, 1H), 7.07–6.96 (m, 2H), 6.86 (s, 1H), 6.62 (s, 1H), 6.29 (d, 1H, J = 3.20 Hz), 3.96 (s, 3H).[1, 2]

1.2. Compound An-B-2OMe. Compound **Mp-py** (346 mg, 2 mmol) was dissolved in anhydrous THF (25 mL), stirred for 30 min under nitrogen atmosphere, then 9-Anthraldehyde (206 mg, 1 mmol) was added, and then two drops trifluoroacetic acid were added, stirred for another 30 mins, reacted at room temperature for two hours, then reflux overnight, after cooling to room temperature, DDQ (226 mg, 1 mmol) was dissolved in THF (25 mL) and added dropwise to the reaction system, and then the mixture was heated to reflux overnight. After being cooled to room temperature added triethylamine (5.75 mL) dropwise, after stirring for 30 mins, added trifluoroacetic acid boron ether

complex dropwise (6 mL), refluxed for 4 hours. After the reaction was completed, the solvent was evaporated under reduced pressure to obtain a crude product. The product was purified by column chromatography (silica gel column, DCM : ethyl acetate = 97 : 3 , v/v) to give pure product as red solid (120 mg, yield: 21%). ^{1}H NMR (400 MHz, $CDCl_3$): δ = 8.62 (s, 1H), 8.09–8.05 (m, 4H), 7.90 (d, 2H, J = 7.80 Hz), 7.53–7.46 (m, 4H), 7.38–7.34 (m, 2H), 7.06–7.03 (t, 2H, J = 7.80 Hz), 6.94 (s, 1H), 6.92 (s, 1H), 6.47 (d, 2H, J = 4.20 Hz), 6.27 (d, 2H, J = 4.20 Hz), 3.78 (s, 6H). MALDI–TOF–MS ($C_{37}H_{27}BF_2N_2O_2$): calcd m/z 580.2; found m/z 580.2.[3]

1.3. Compound An-BO. Compound **An-B-2OMe** (58 mg, 0.1 mmol) was dissolved in anhydrous DCM (3.5 mL), BBr_3 (250 mg, 1 mmol, 10 eq) was added dropwise under 0 °C, heated to room temperature and react for 5 hours. After the reaction was completed, it was quenched with water and extracted with dichloromethane (DCM), The organic layer was separated and washed with water and brine solution, respectively. The organic layer was dried over anhydrous Na_2SO_4 and the solvent was evaporated under reduced pressure. The product was purified by column chromatography (silica gel column, petroleum ether : ethyl acetate = 4 : 1 , v/v) to give pure product as dark red solid (25 mg, yield: 49%) ^{1}H NMR (400 MHz, $CDCl_3$): δ = 8.63 (s, 1H), 8.08 (d, 2H, J = 8.87 Hz), 7.91 (d, 2H, J = 8.87 Hz), 7.80 (d, 2H, J = 8.87 Hz), 7.50–7.47 (m, 2H), 7.42–7.35 (m, 4H), 7.11–7.05 (m, 4H), 6.77 (d, 2H, J = 4.30 Hz), 6.52 (d, 2H, J = 4.30 Hz). ^{13}C NMR (126 MHz, $CDCl_3$): δ =154.28, 150.43, 136.62, 135.40, 132.43, 131.34, 131.02, 129.04, 128.91, 128.35, 126.55, 126.46, 126.40, 125.98, 125.55, 120.58, 119.90, 119.72, 116.31, MALDI–TOF–HRMS ($C_{35}H_{21}BN_2O_2$): calcd m/z 512.1696; found m/z 512.1707.[4]

2. NMR, HRMS Spectra

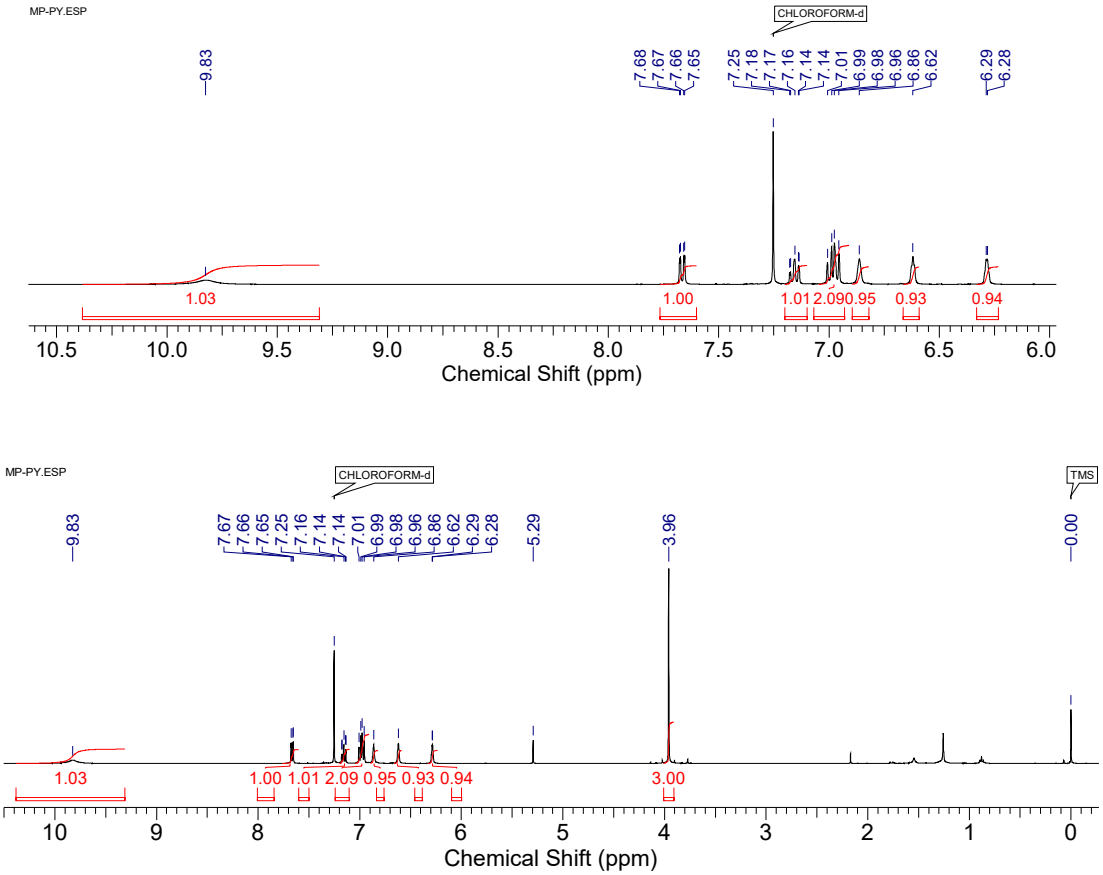

Fig. S1 ^{1}H NMR spectrum of compound **Mp-py** (400 MHz, $CDCl_3$), 25 °C.

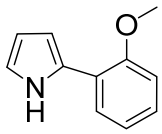

Mp-py

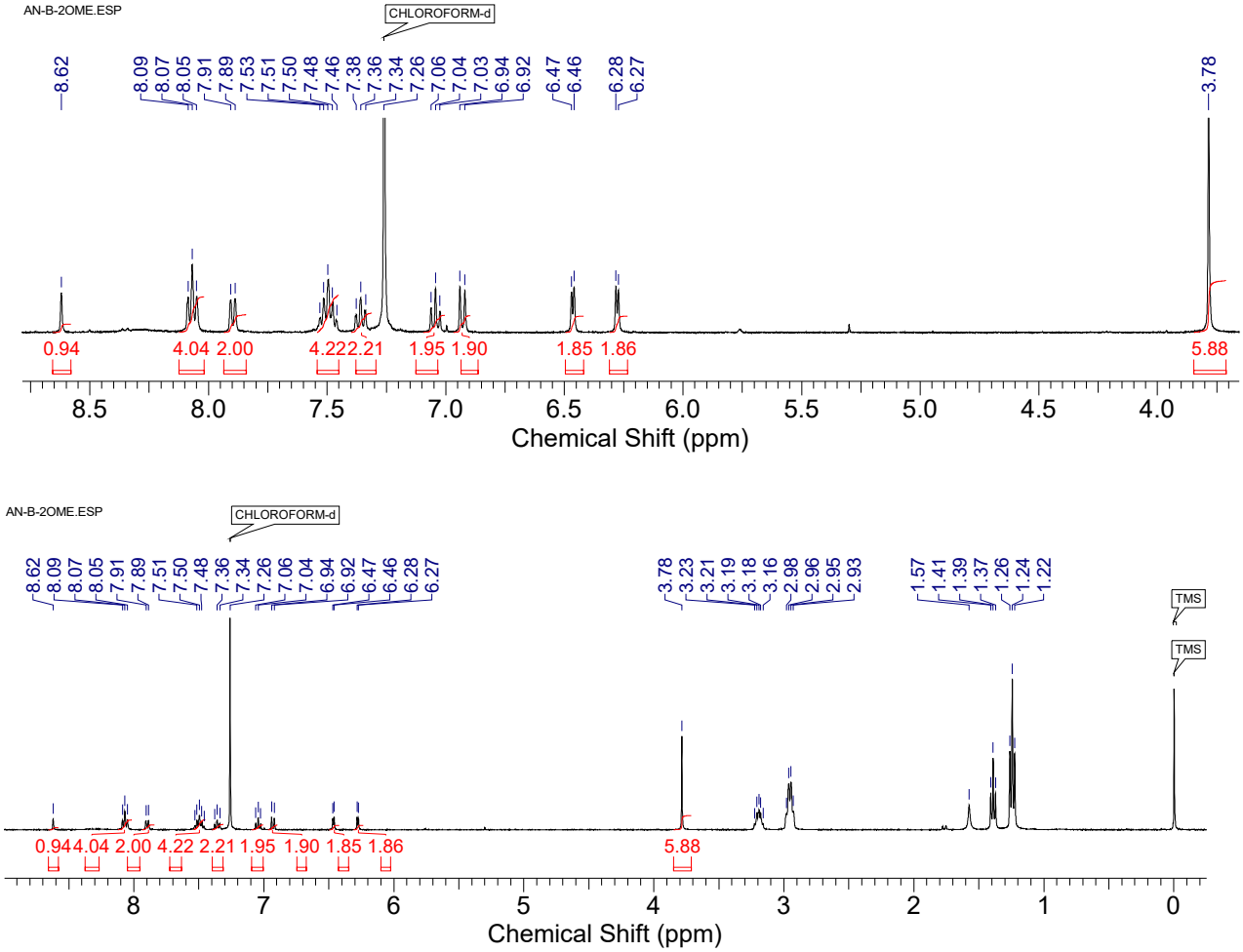

Fig. S2 ^{1}H NMR spectrum of compound **An-B-2OMe** (400 MHz, $CDCl_3$), 25 °C.

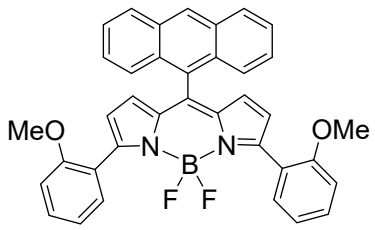

An-B-2OMe

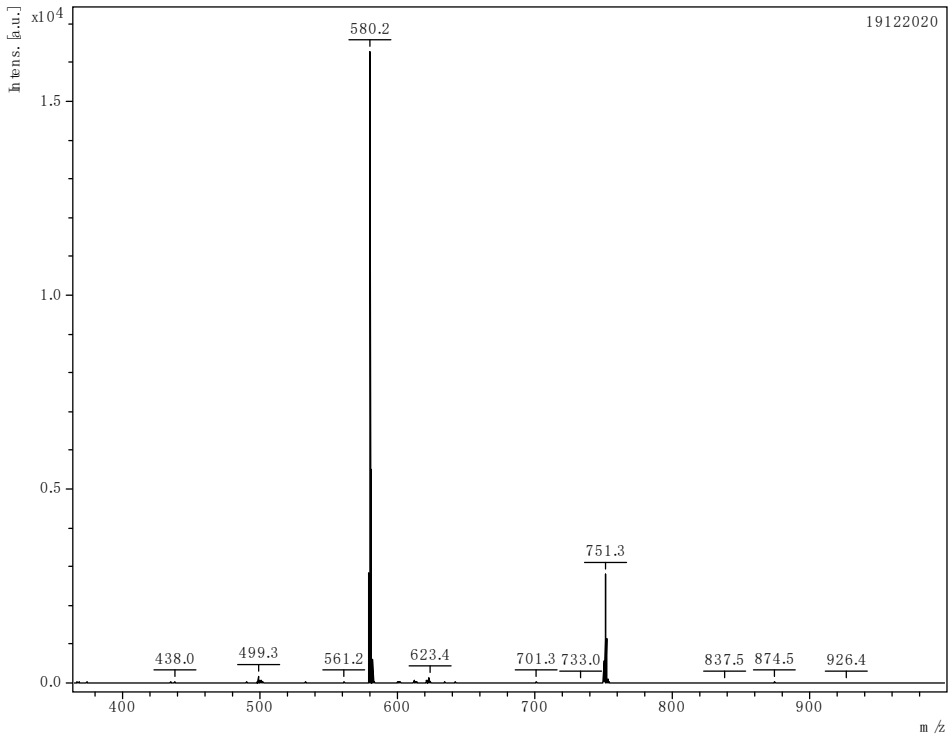

Fig. S3 MALDI–TOF–MS of compound **An-B-2OMe**, 25 °C.

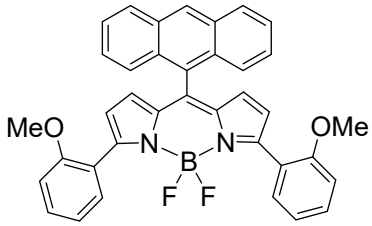

An-B-2OMe

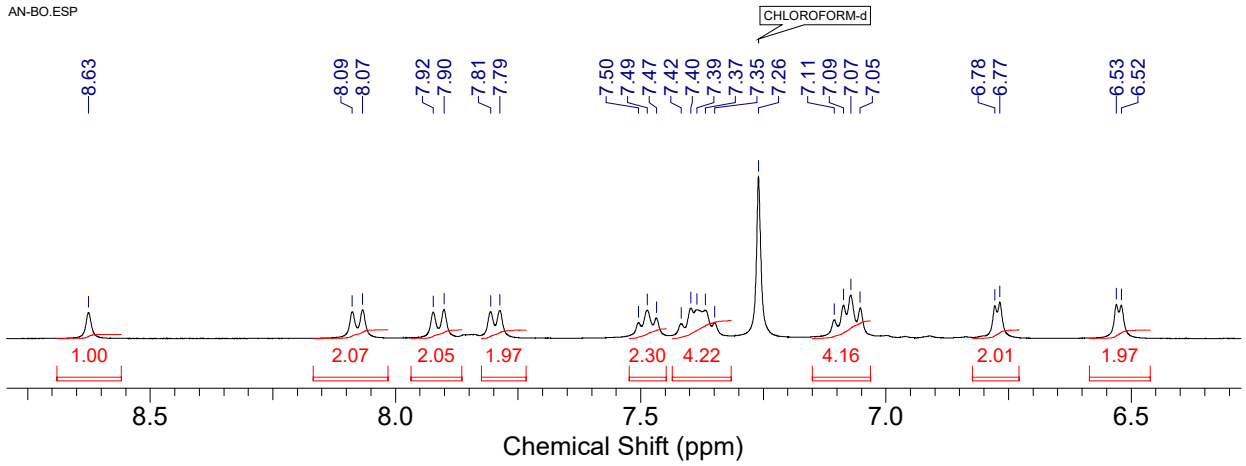

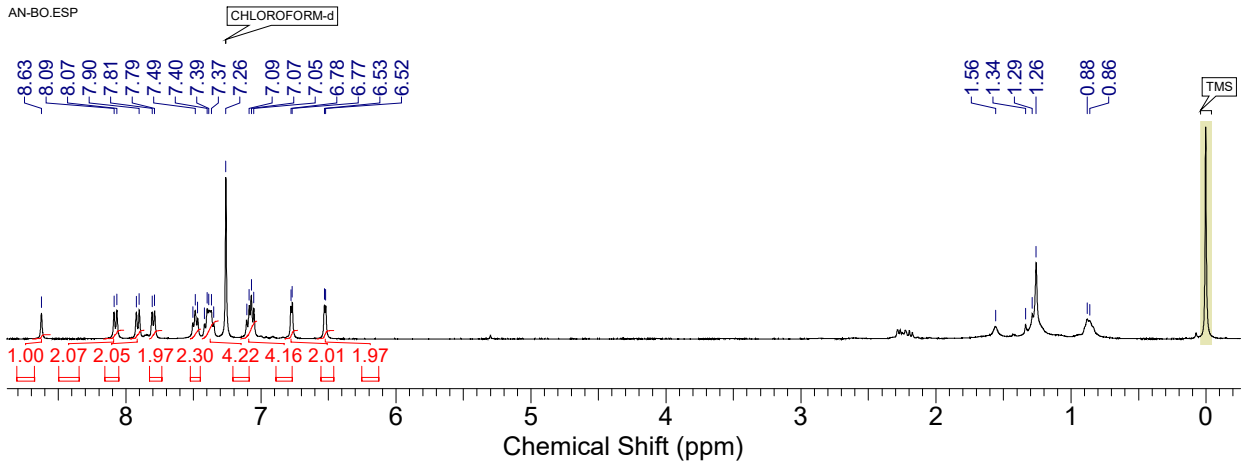

Fig. S4 ^{1}H NMR spectrum of compound **An-BO** (400 MHz, $CDCl_3$), 25 °C.

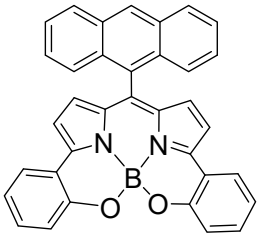

An-BO

Formula	Mass	Error	mSigma	DblEq	N rule	Electron Configuration
C 35 H 21 B N 2 O 2	512.1696	2.1098	32.5370	27.00	ok	odd

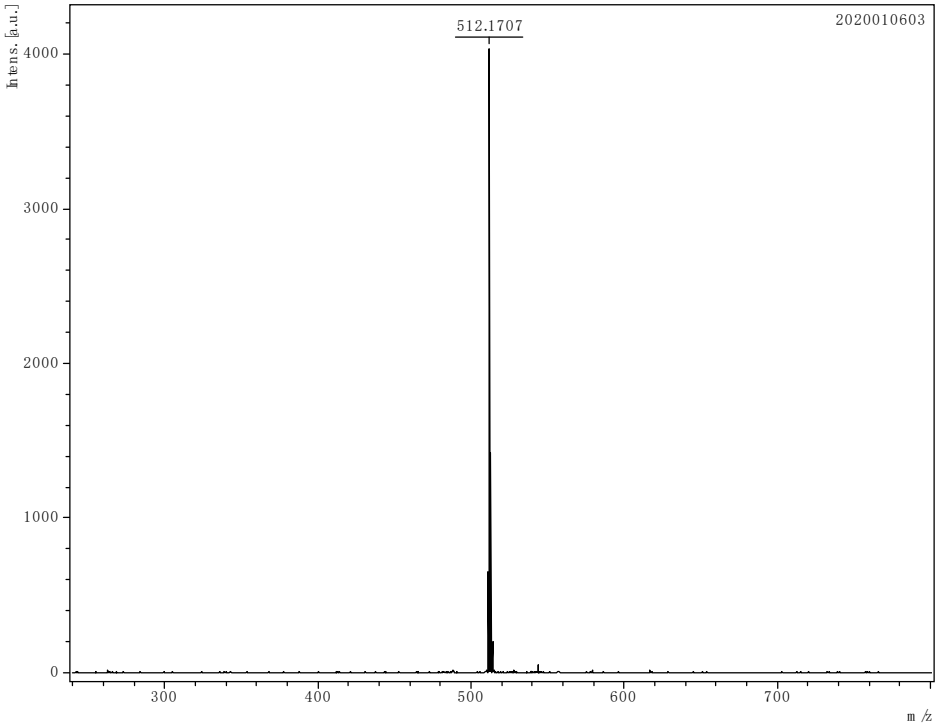

Fig. S5 MALDI–TOF–HRMS of compound **An-BO**, 25 °C.

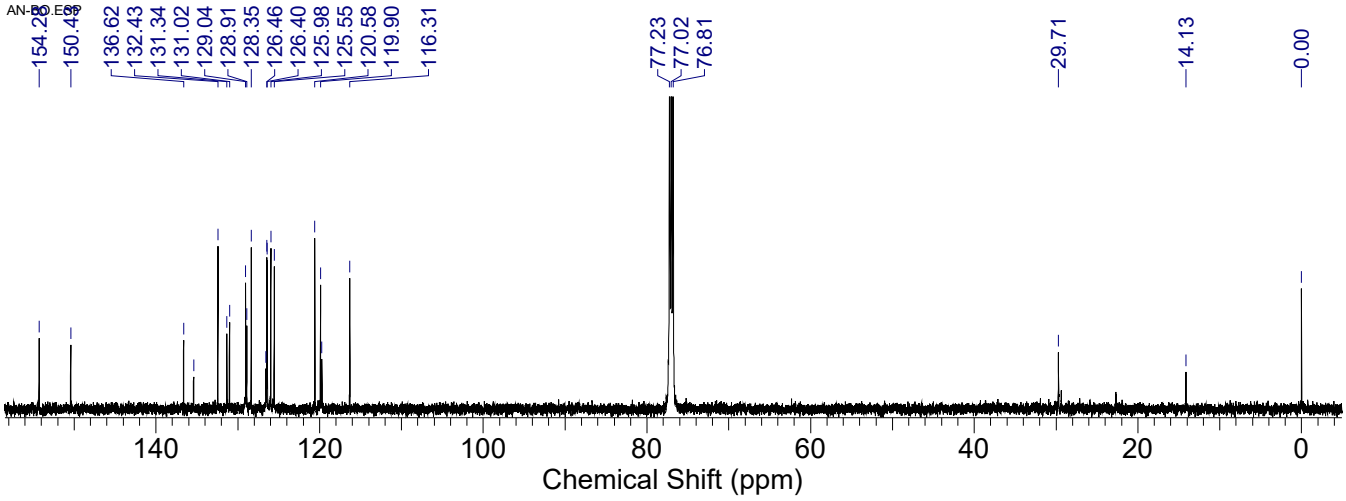

Fig. S6 ^{13}C NMR spectrum of compound **An-BO** (151 MHz, $CDCl_3$), 25 °C.

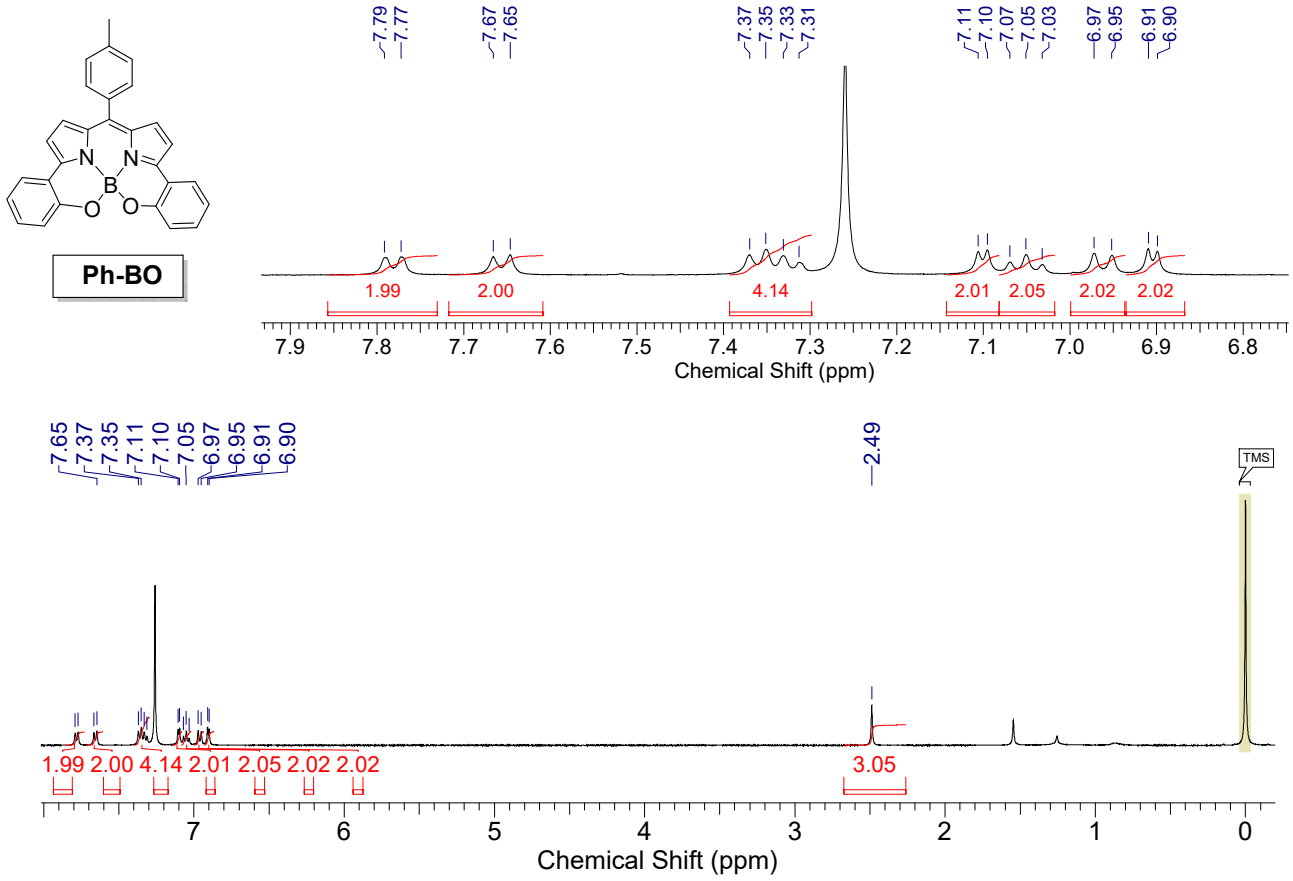

Fig. S7 ^{1}H NMR spectrum of compound **Ph-BO** (400 MHz, $CDCl_3$), 25 °C.

SmartFormula

Formula	Mass	Error	mSigma	DblEq	N rule	Electron Configuration
C 28 H 19 B N 2 O 2	426.1534	4.8060	49.5980	21.00	ok	odd

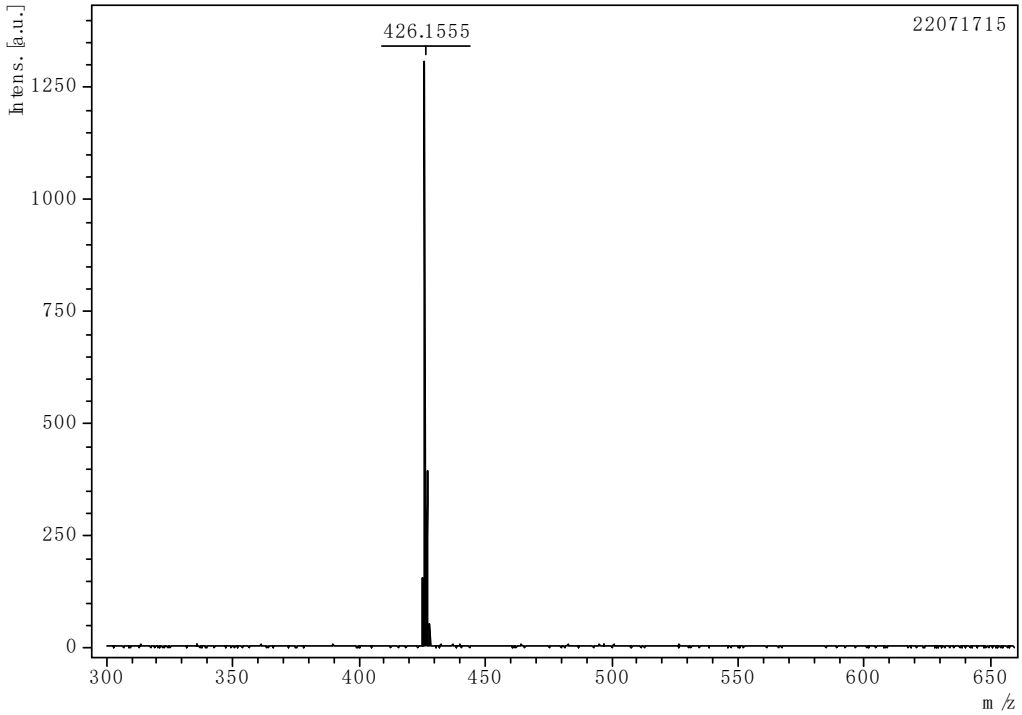

Fig. S8 MALDI–TOF–HRMS of compound **Ph-BO**, 25 °C.

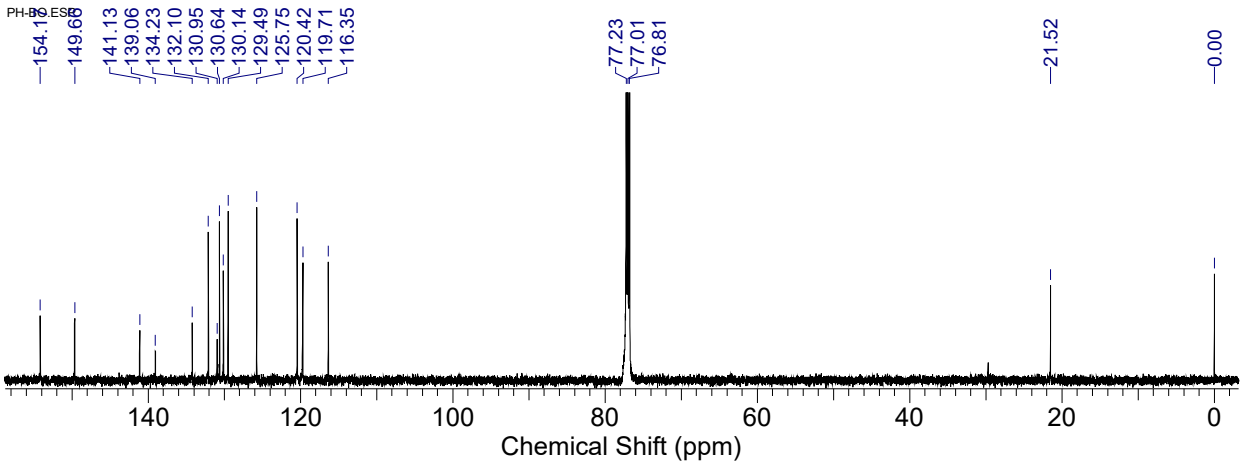

Fig. S9 ^{13}C NMR spectrum of compound **Ph-BO** (151 MHz, $CDCl_3$), 25 °C.

3. Crystallographic Data

Table S1. Crystallographic Data for **Ph-BO**.

Compound	**Ph-BO**
Empirical formula	C_{28} H_{19} B N_2 O_2
M (g mol^{-1})	426.26
Temperature / K	200 K
Crystal system	triclinic
Space group	P-1
a (Å)	7.9377(10)
b (Å)	9.5122(12)
c (Å)	14.8507(19)
α (deg)	97.129(3)
β (deg)	98.579(3)
γ (deg)	105.788(3)
Volume / Å^3	1050.8(2)
Z	2
D_{calc} / g · cm^{-3}	1.347
F (000)	444.0
μ (Mo – Kα) / mm^{-1}	0.085
2Θ range for data collection/°	4.518 to 55.28
Reflections collected	22543
Independent reflections	4893 [R_{int} = 0.0969, R_{sigma} = 0.0969]
Data/restraints/parameters	4893/0/299
Largest diff. peak and hole (e Å^{-3})	0.28/–0.30
Goodness of fit	1.025
Final R indexes [I>=2σ (I)]	R_1 = 0.0659, wR_2 = 0.1116
Final R indexes [all data]	R_1 = 0.1459, wR_2 = 0.1362

4. UV/Vis Absorption Spectra

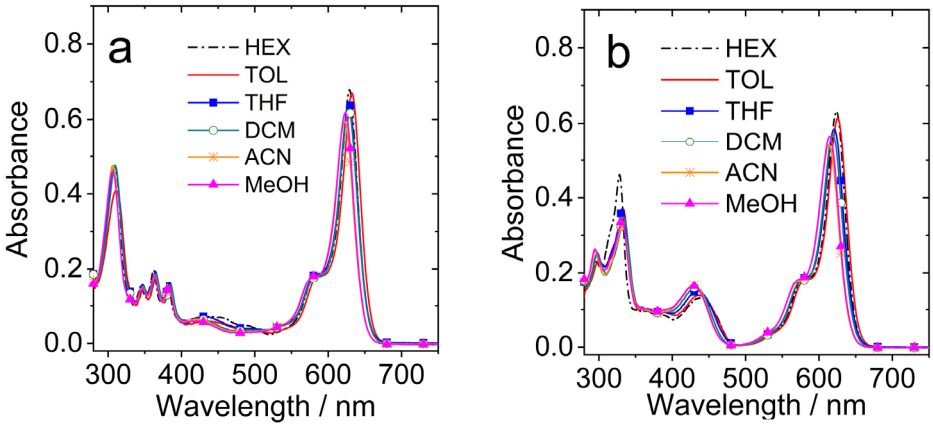

Fig. S10 UV/Vis absorption spectra of the (a) **An-BO** and (b) **Ph-BO** in different solvents. c = 1.0 × 10^{-5} M, 25 °C. 'HEX' stand for *n*-hexane, 'TOL' stand for toluene, 'THF' stand for tetrahydrofuran, 'DCM' stand for dichloromethane, 'ACN' stand for acetonitrile and 'MeOH' stand for methanol.

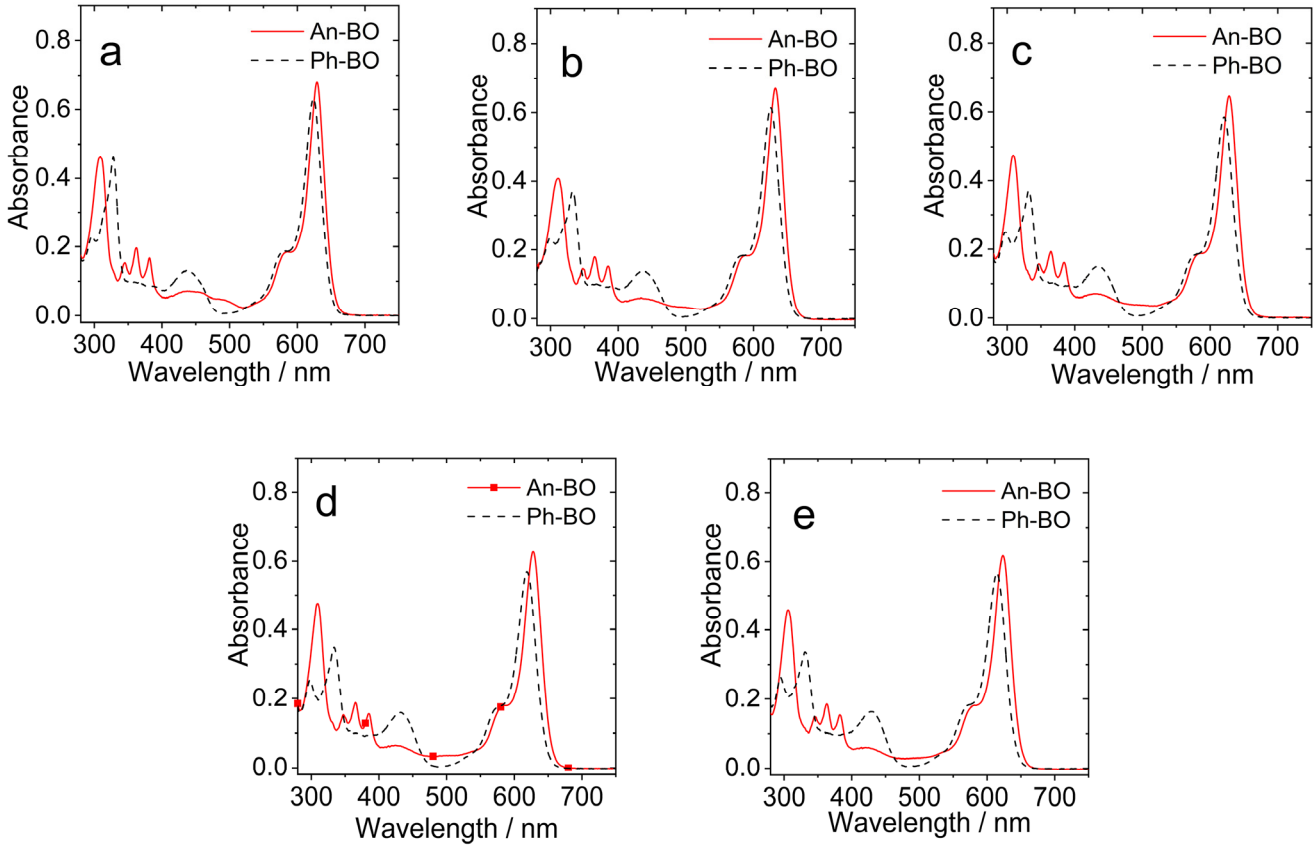

Fig. S11 UV/Vis absorption spectra of the compounds in (a) *n*-hexane, (b) toluene, (c) tetrahydrofuran, (d) dichloromethane and (e) methanol c = 1.0 × 10^{-5} M, 25 °C.

5. Fluorescence Spectra

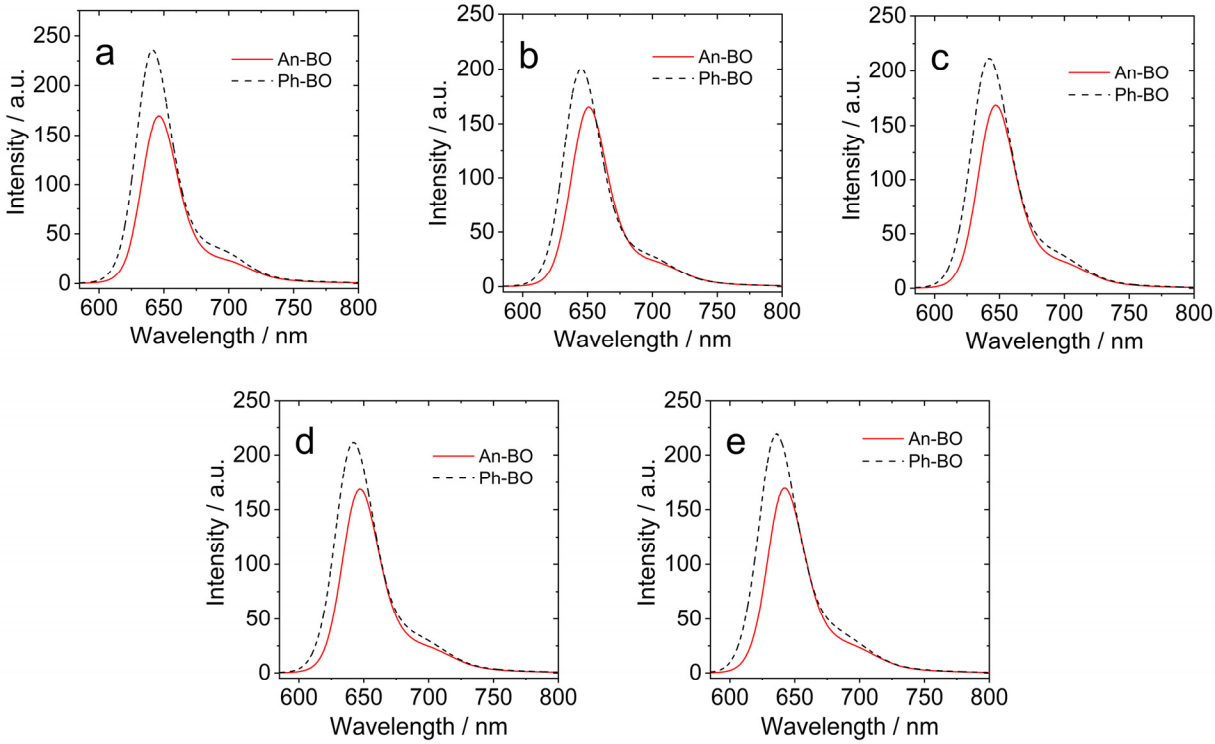

Fig. S12 Fluorescence spectra of the compounds in (a) *n*-hexane, (b) toluene, (c) tetrahydrofuran, (d) dichloromethane and (e) methanol, λ_{ex} = 580 nm. Optically matched solutions were used in each panel (each of the solutions gives the same absorbance at the excitation wavelength, A = 0.100), 25 °C.

6. Fluorescence Lifetime

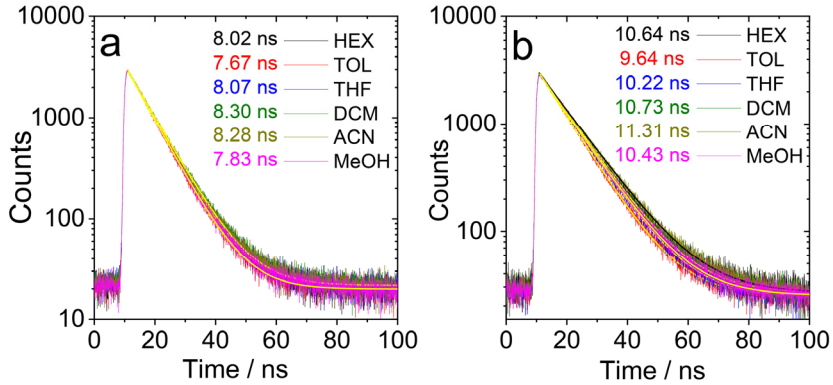

Fig. S13 Fluorescence decay trances of (a) **An-BO** and (b) **Ph-BO** in different solvents. Excited with picosecond EPL laser (λ_{ex} = 610 nm), the fluorescence decay traces were monitored at 650 nm, c = 1.0 × 10^{-5} M, 25 °C.

7. Cyclic Voltammograms

$$\Delta G_{CS} = e[E_{OX} - E_{RED}] - E_{00} + \Delta G_S \quad \text{(S1)}$$

$$\Delta G_S = -\frac{e^2}{4\pi\varepsilon_s\varepsilon_0 R_{CC}} - \frac{e^2}{8\pi\varepsilon_0}\left(\frac{1}{R_D} + \frac{1}{R_A}\right)\left(\frac{1}{\varepsilon_{REF}} - \frac{1}{\varepsilon_S}\right) \quad \text{(S2)}$$

$$E_{CS} = e[E_{OX} - E_{RED}] + \Delta G_S \quad \text{(S3)}$$

For Eq S1–S3, ΔG_{CS} is the Gibbs free-energy change of charge separation process, e is the charge of a single electron, E_{RED} and E_{OX} are the half-wave potential for one-electron reduction and oxidation of the electron-acceptor unit, respectively, E_{00} represent the energy level approximated with the crossing point of UV/Vis absorption and fluorescence emission after normalization at the singlet excited state. ΔG_S is the static coulombic energy, ε_s is the static dielectric constant of the

solvent, ε_0 is the permittivity of free space, R_{CC} is the center-to-center separation distance between the electron donor and acceptor determined by optimized conformation by DFT calculation, R_D and R_A are the radius of electron donor and acceptor, ε_{REF} is the static dielectric constant of the solvent used for the electrochemical studies and E_{CS} is charge separation state energy level.

8. Femtosecond Transient Absorption Spectroscopy.

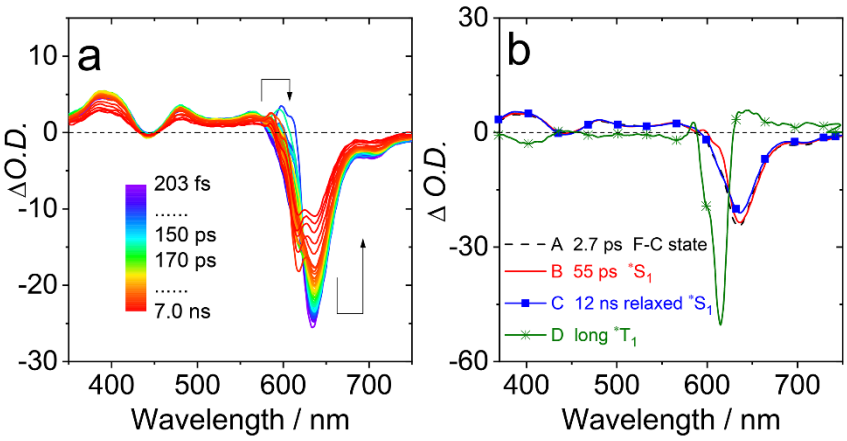

Fig. S14 (a) Femtosecond transient absorption spectra of **Ph-BO** recorded in *n*-hexane, the relative SADS obtained with global analysis are presented in panel (b). λ_{ex} = 610 nm, $c = 1 \times 10^{-5}$ M.

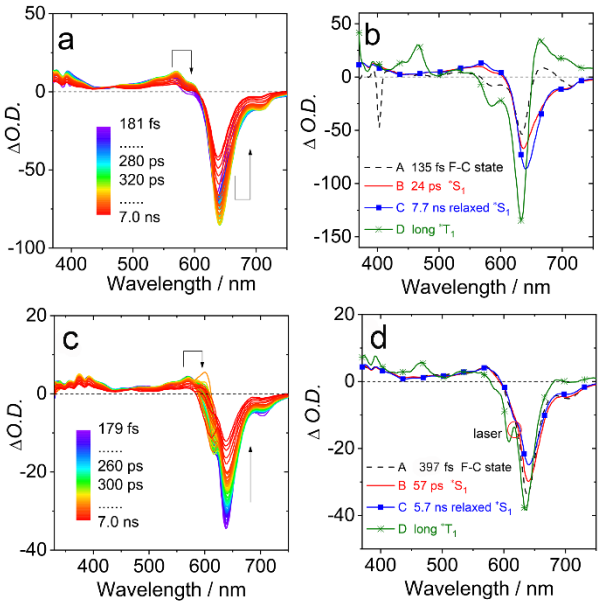

Fig. S15 Femtosecond transient absorption spectra of **An-BO** recorded in *n*-hexane excited at (a) 360 nm and (c) 610 nm, the relative SADS obtained with global analysis are presented in panel (b) and in panel (d), respectively, $c = 1 \times 10^{-5}$ M.

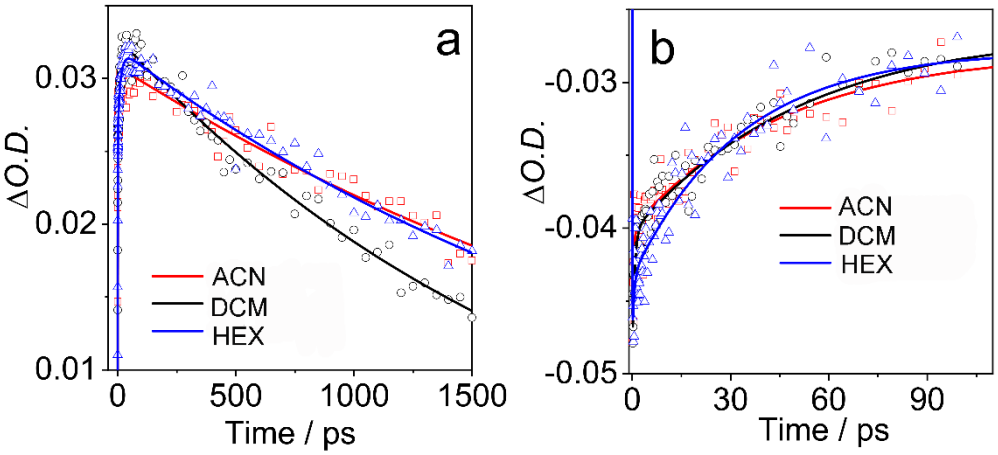

Fig. S16 Comparison at early time delays between the kinetic traces at 630 nm of (a) **An** and (b) **Ph-BO** in different solvent, ACN (red trace), DCM (black trace) and HEX (blue trace).

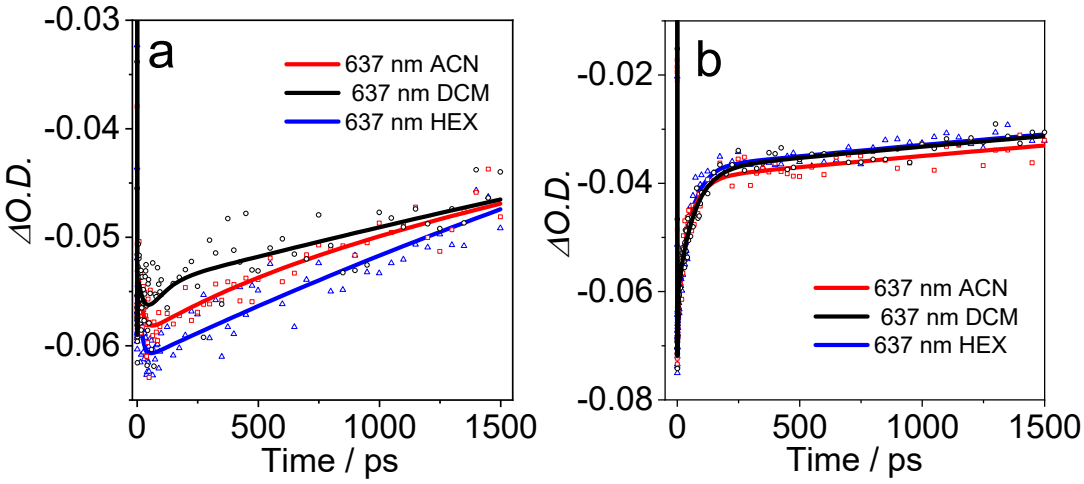

Fig. S17 Comparison between the kinetic traces at GSB band (637 nm) of **An-BO** recorded after the excitation at (a) 360 nm and (b) 610 nm, in the three different solvents: hexane (blue trace), dichloromethane (black trace) and acetonitrile (red trace).

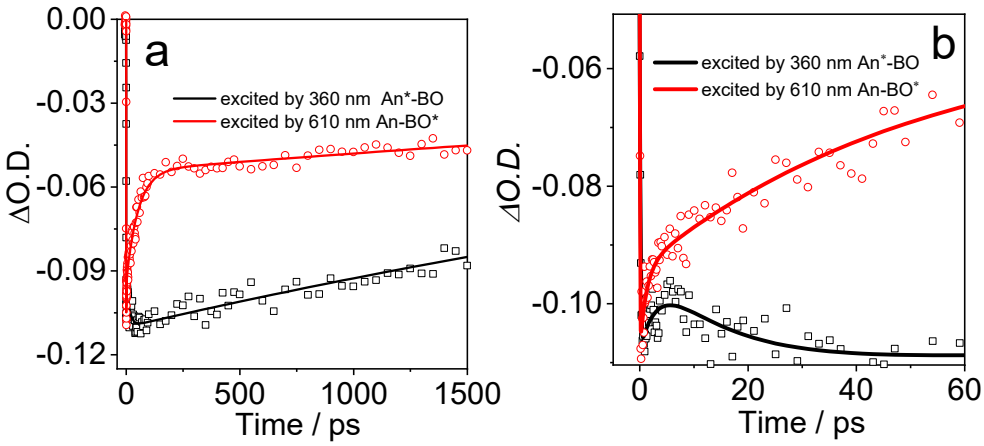

Fig. S18 Comparison between the kinetic traces at 637 nm of **An-BO** in hexane recorded after the excitation at 610 nm (red trace) and after the excitation at 360 nm (black trace) in different time range (a) 1.5 ns and (b) 60 ps detail of the kinetic traces at early time delays is reported.

9. Nanosecond Transient Absorption Spectra.

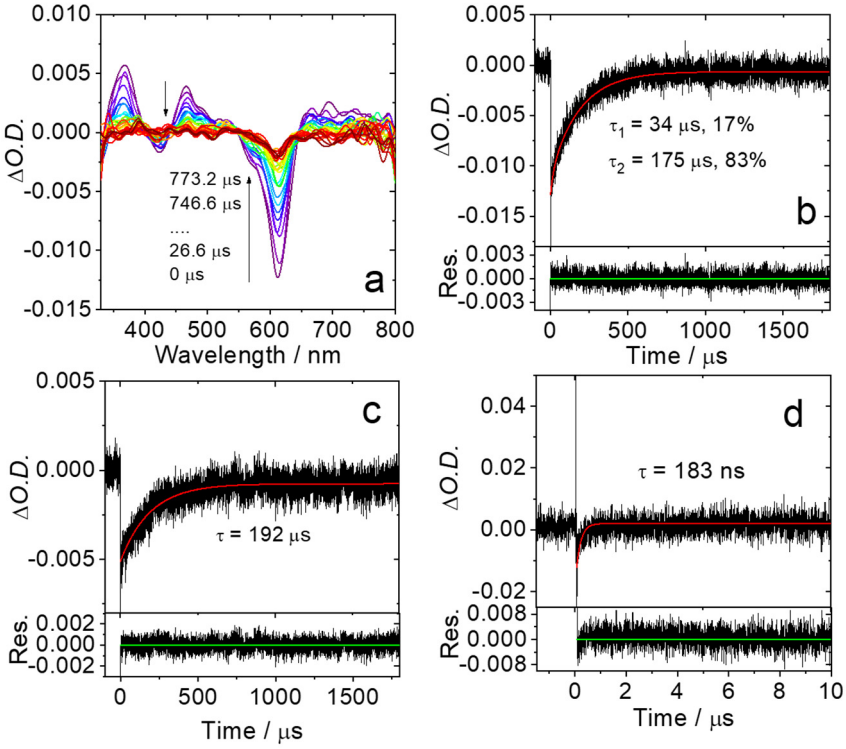

Fig. S19 (a) Nanosecond time-resolved transient absorption spectra of **Ph-BO** upon pulsed laser excitation (λ_{ex} = 610 nm), decay trace of **Ph-BO** at 605 nm in (b) deaerated and (d) aerated acetonitrile, c = 1 × 10^{-5} M. (c) Decay trace of **Ph-BO** at 605 nm in deaerated acetonitrile, c = 5 × 10^{-6} M, 25 °C.

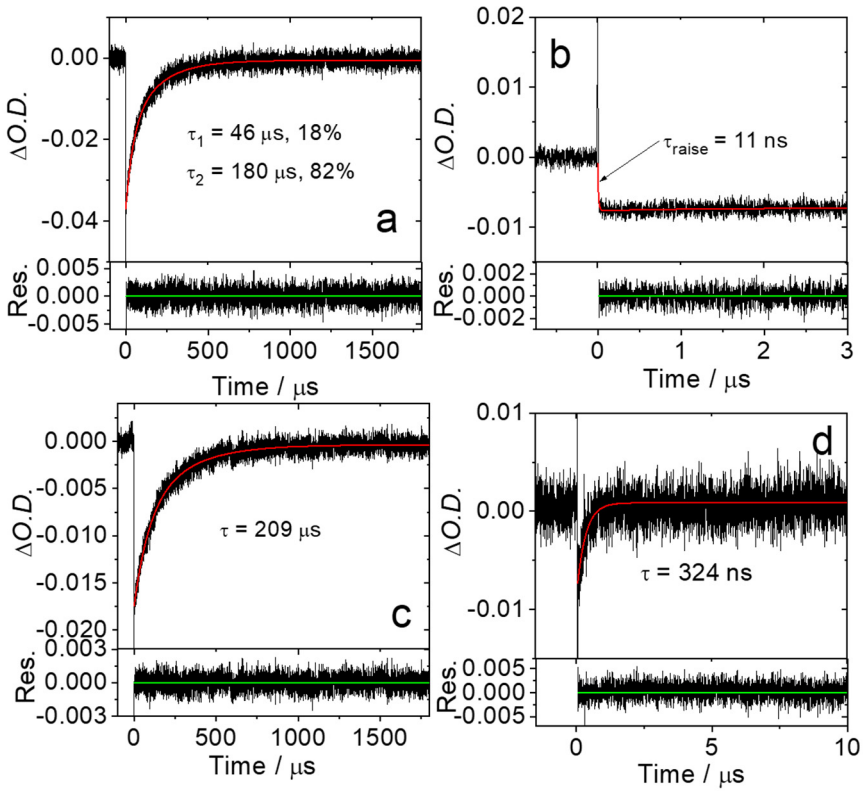

Fig. S20 Decay trace of **An-BO** at 605 nm in deaerated acetonitrile in (a) long time range and (b) short time range, triplet state formation was observed, c = 1 × 10^{-5} M. (c) Decay trace of **An-BO** at 605 nm in deaerated acetonitrile, c = 5 × 10^{-6} M. (d) Decay trace of **An-BO** at 605 nm in aerated acetonitrile. c = 1 × 10^{-5} M, 25 °C.

Intrinsic triplet state lifetime fitting:[5]

When the intrinsic triplet state lifetime is long and the triplet state quantum yield is high, the triplet-triplet annihilation will contribute additional lifetime quenching factor to the decay of the transient absorption. Then triplet state lifetime will be quenched significantly and the experimental values will be shorter than the intrinsic lifetime. The corresponding differential equation for the triplet concentration

$$\frac{dc_T}{dt} = -k_1 c_T - k_2 c_T^2 \tag{S4}$$

has the solution

$$c_T(t) = \frac{c_0 k_1}{exp(k_1 t)\cdot(c_0 k_2 + k_1) - c_0 k_2} \quad \text{(S5)}$$

Where c_0 is the initial triplet concentration. This leads to the following expression for the transient absorption

$$A(t) = \frac{A_0\, \tau_2/\tau_1}{exp(t/\tau_1)\cdot(1+\tau_2/\tau_1)-1} \quad \text{(S6)}$$

Where A_0 is the initial transient absorption, $\tau_1 = 1/k_1$ is the intrinsic (unimolecular) lifetime of the triplet, and $\tau_2 = 1/c_0 k_2$. We fitted the data sets of **An-BO** and **Ph-BO** triplet state lifetime values simultaneously by Eq. S6, with variation of all parameters (A_0, τ_1, τ_2), but with the intrinsic triplet lifetime constrained to the same value in all data sets.

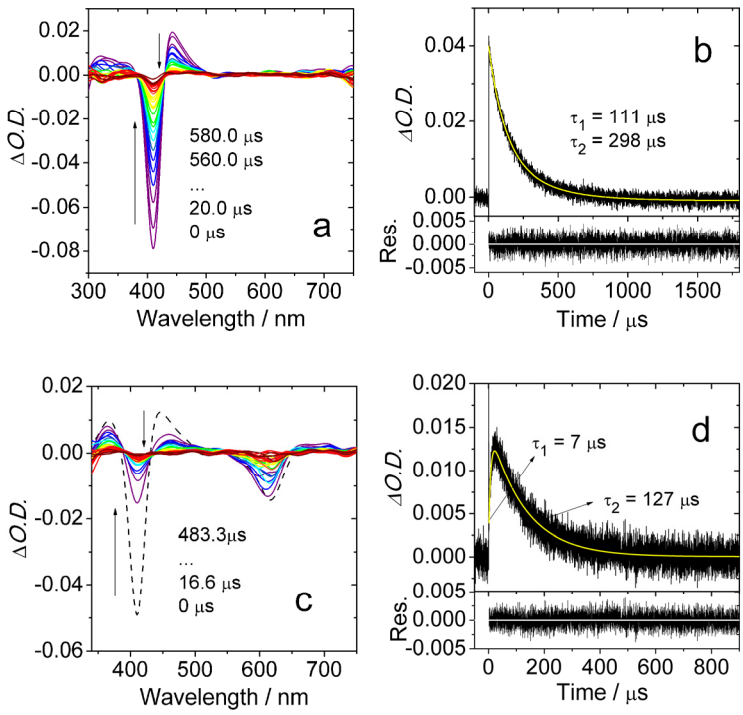

Fig. S21 (a) Nanosecond time-resolved transient absorption spectra of TPP upon pulsed laser excitation (λ_{ex} = 415 nm) use co-linear mode, (b) decay trace of TPP at 420 nm in c = 3.0 × 10^{-6} M, (c) intermolecular triplet energy transfer with TPP as the triplet energy donor and **Ph-BO** as the triplet energy acceptor, studied with nanosecond transient absorption spectra and (d) the decay trace at 610 nm, c [TPP] = 3.0 × 10^{-6} M, c [**Ph-BO**] = 2.0 × 10^{-5} M. λ_{ex} = 415 nm, in deaerated acetonitrile, 25 °C.

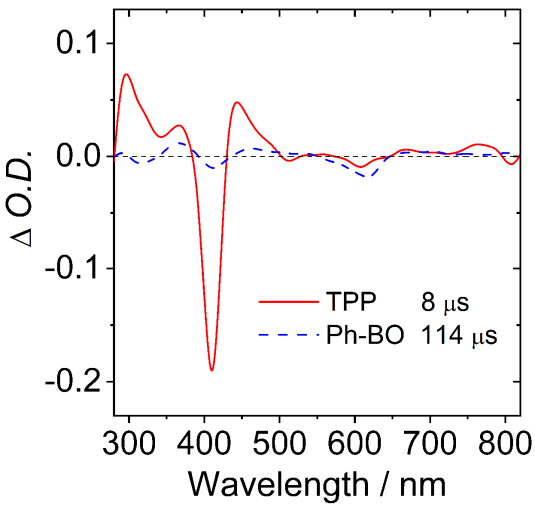

Fig. S22 The species-associated difference spectra (EADS) of the mixture, the raw data is from Fig. S22c.

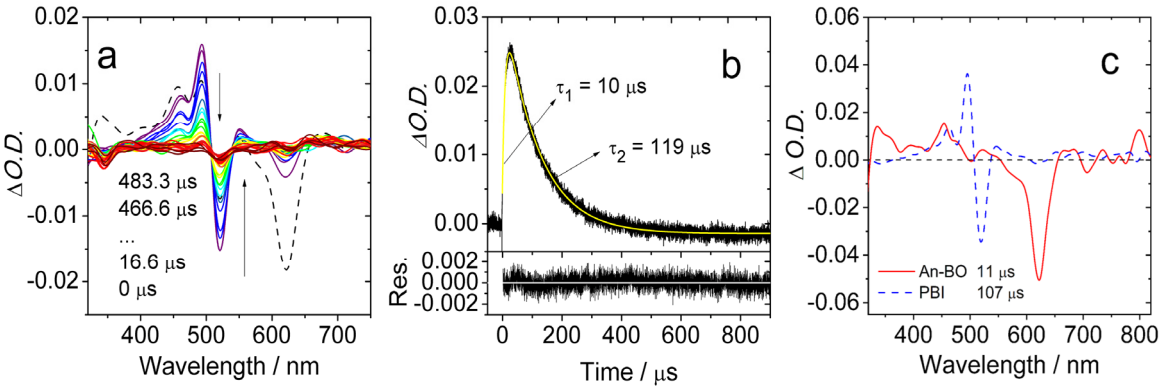

Fig. S23 (a) Intermolecular triplet energy transfer with **An-BO** as the triplet energy donor and **PBI** as the triplet energy acceptor, studied with nanosecond transient absorption spectra, (d) the decay trace at 500 nm and (c) the species-associated difference spectra (EADS) of the mixture, the raw data is from (a), c [**An-BO**] = 5.0 × 10^{-6} M, c [**PBI**] = 2.0 × 10^{-5} M. λ_{ex} = 610 nm, in deaerated acetonitrile, 25 °C.

10. Time-resolved Electron Paramagnetic Resonance Spectroscopy

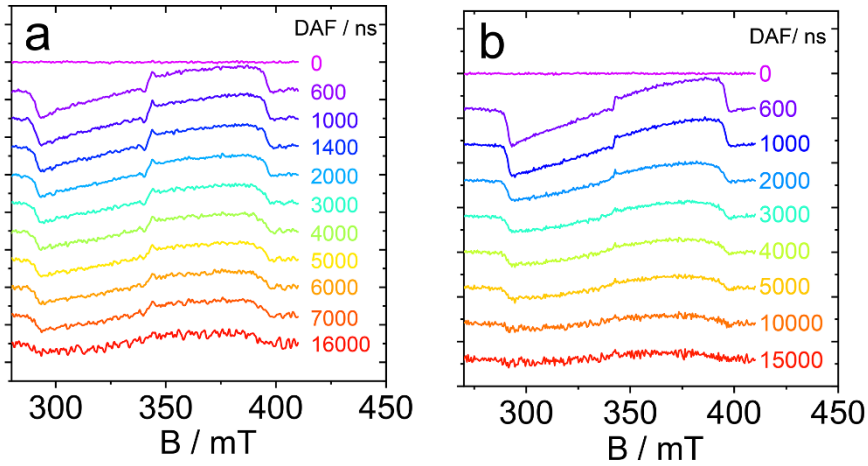

Fig. S24 TR EPR spectra of (a) **An-BO** with concetration 3×10^{-4} M, the frozen samples were photo-excited at 585 nm with pulse laser at energies of 1 mJ. (b) **Ph-BO** with concetration 2×10^{-4} M, the frozen samples were photo-excited at 613 nm with pulse laser at energies of 1 mJ. Sample was dissolved in Toluene/2–MeTHF (1/1, v/v) at 80 K.

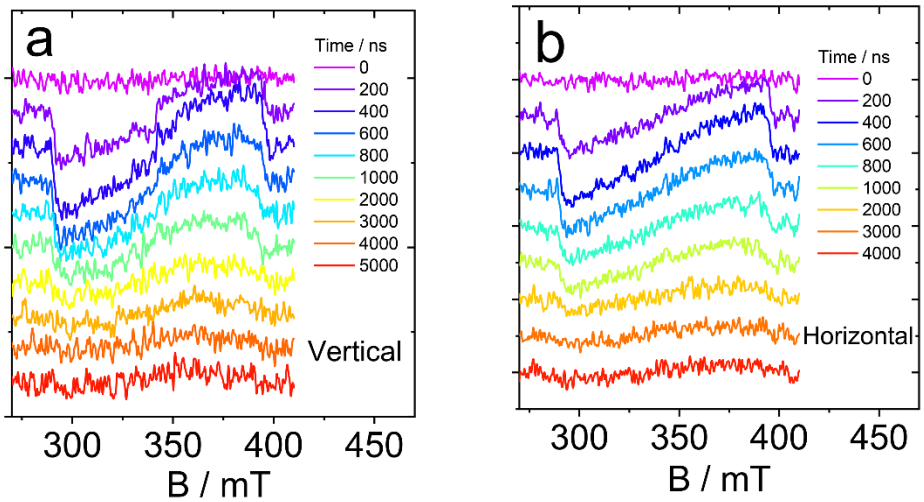

Fig. S25 Magnetophotoselection TREPR spectra of **Ph-BO.** (a) The polarization of the laser is perpendicular to the magnetic field direction; (b) The polarization of the laser is parallel to the magnetic field direction. The frozen samples were photo-excited at 532 nm with pulse laser at energies of 10 mJ, 80 K.

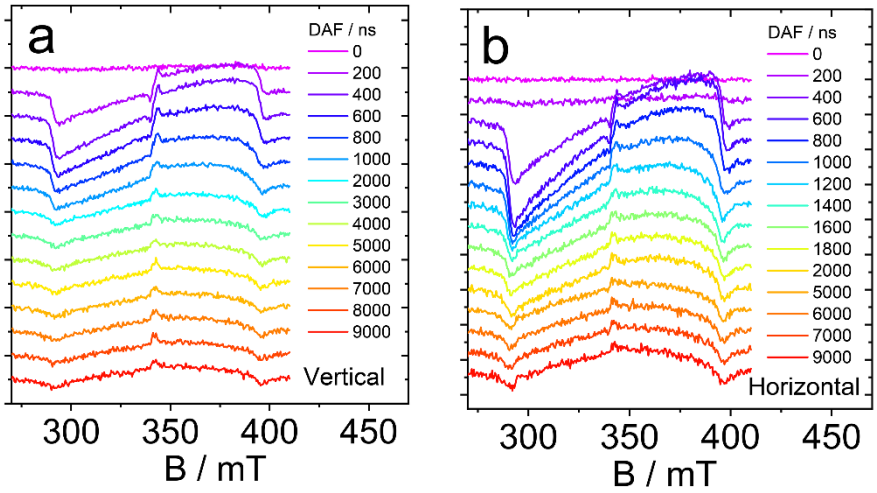

Fig. S26 Magnetophotoselection TREPR spectra of **An-BO.** (a) The polarization of the laser is perpendicular to the magnetic field direction; (b) The polarization of the laser is parallel to the magnetic field direction. The frozen samples were photo-excited at 532 nm with pulse laser at energies of 10 mJ, 80 K. Polarization for the magnetophotoselection experiments was obtained using a Glan laser polarizer (SolarLS) in combination with a half-wave plate.

11. Theoretical Computations

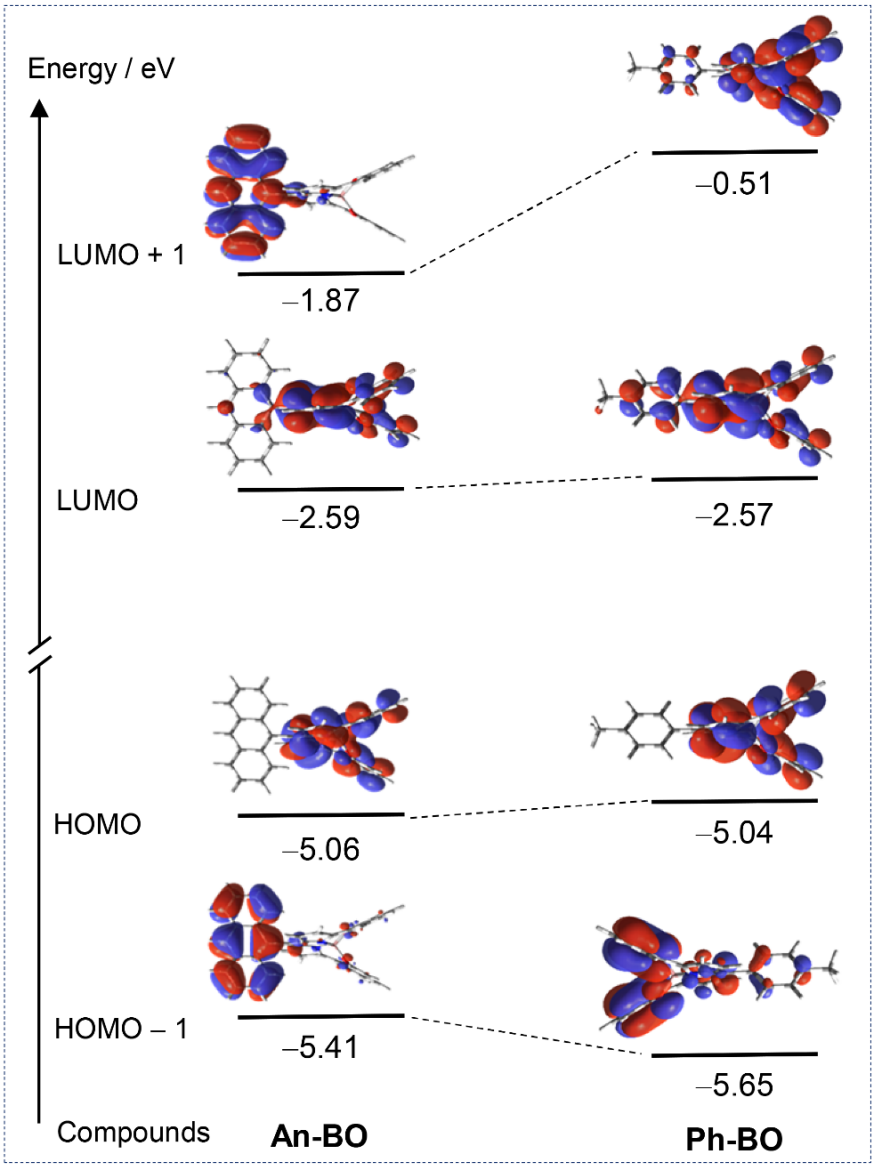

Fig. S27 Selected frontier molecular orbitals of **An-BO** and **Ph-BO** calculated at DFT (CAM-B3LYP/6-31G (d)) level with Gaussian 09W. The energy levels of the orbits are also presented (in eV). Iso value of the molecular orbitals surfaces is 0.0004.

Table S2. Energies above the optimized S_0 state (in cm^{-1}) of the lowest singlet and triplet states at the optimized geometries indicated in the column header, calculated with TD-DFT and the CAM-B3LYP functional.[a]

	An-BO					**Ph-BO**				**BO**			
	S_0-g	S_1-g	T_1-g	T_2-g	T_3-g	S_0-g	S_1-g	T_1-g	T_2-g	S_0-g	S_1-g	T_1-g	T_2-g
S_0	0	722	766	2681	1400	0	699	1031	1917	0	648	1061	1920
S_1	21477	20718	20962	23631	21375	21361	20640	21043	21480	21609	20940	21364	22079
T_1	11709	11134	10859	14135	11863	11923	11387	11138	12438	11527	10983	10736	12246
T_2	17548	17755	17965	14629	17704	21900	20771	21304	19907	22603	21663	22139	20664
T_3	22488	21064	21417	22688	20383								

[a] S_x-g respect for at the S_x optimized geometries.

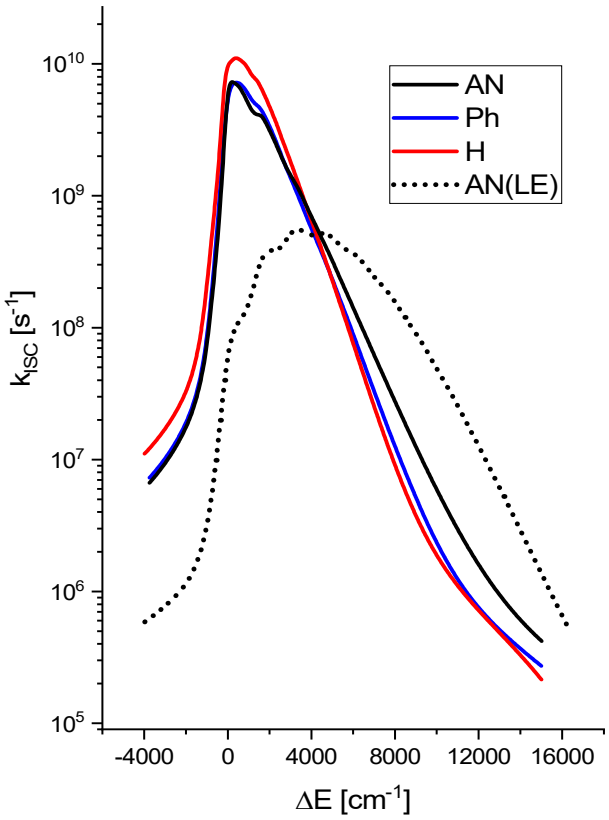

Fig. S28 Energy gap dependence of the ISC rate constant for $S_1 \rightarrow T_n$ transitions. The full lines are for the second local triplet of the **BO** unit, which is T_2 in BO and **Ph-BO** and T_3 in An-BO. The dotted line is for T_2 of **An-BO** which is a local triplet on the An unit. The second local triplet on the BO unit is probably higher than the S_1 state, i.e. the energy gap is negative. A gap in the range – (1500 – 1000) cm^{-1} would still allow ISC with rate constants of ca. 10^8 s^{-1}.

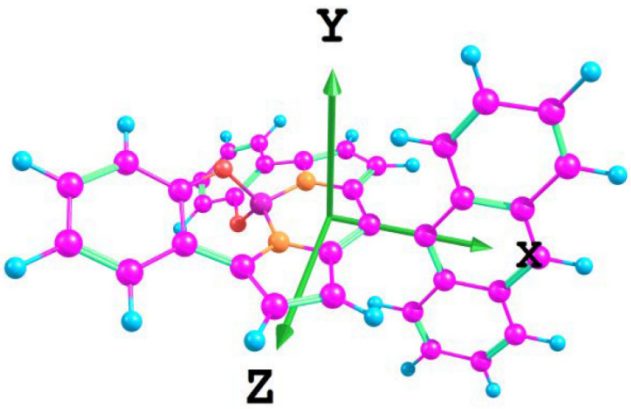

Fig. S29 The calculated ISC rates for the three triplet substates individually. The coordinate system of the ZFS tensor is determined by ORCA. In this coordinate system, the molecule is oriented as the X-axis is the twofold symmetry axis of the molecule, and the Z-axis is along the long axis of the BDP chromophore. With this orientation, the following rated for the transitions to the X, Y, Z-states of the triplet were computated.

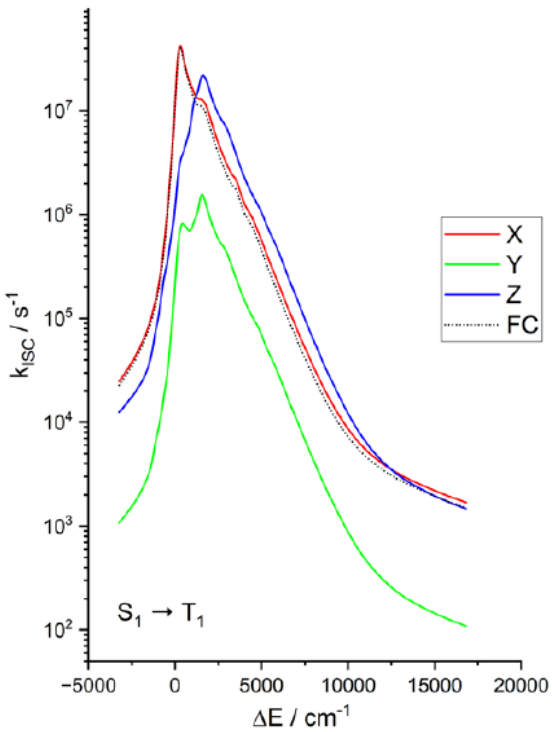

Fig. S30 The computated relations between the intersystem crossing rates to the Tx, Ty and Tz substates of the T_1 state of **Ph-BO** and the energy gap. The dotted line is the pure Franck-Condon (FC) contribution. This leads to the X-component for both transition (T_1 and T_2). The total rate for the $S_1 \rightarrow T_n(X)$ transitions, including the Herzberg Teller (HT) terms, is given by the red line. For T_1 this is almost identical with the FC term, i.e. here the HT contribution is small. For the T_2 sate the HT contribution grows with increasing energy gap. Interestingly, the largest contribution is for the transition to the Z-component of T_2 (blue line), which is entirely due to HT. This is in excellent agreement with the experiment. For the T_1 state, the Z-rate is largest for energy gaps larger than ca. 2000 cm^{-1}, which also agrees with experiment.

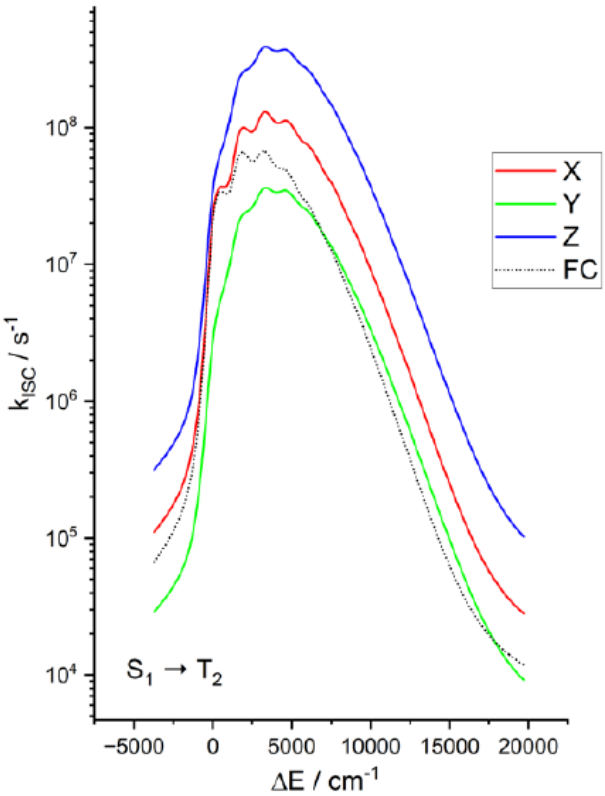

Fig. S31 The computated relations between the intersystem crossing rates to the Tx, Ty and Tz substates of the T_2 state of **Ph-BO** and the energy gap. For other information, please see the captions of Fig. S30.

References

1. R. D. Rieth, N. P. Mankad, E. Calimano and J. P. Sadighi, *Org. Lett.*, 2004, **6**, 3981–3983.
2. L. Copey, L. Jean-Gérard, E. Framery, G. Pilet and B. Andrioletti, *Eur. J. Org. Chem.*, 2014, 4759–4766.
3. X.-Y. Zhu, H. Wu, X.-F. Guo and H. Wang, *Dyes. Pigments*, 2019, **165**, 400–407.
4. R. B. Alnoman, S. Rihn, D. C. O'Connor, F. A. Black, B. Costello, P. G. Waddell, W. Clegg, R. D. Peacock, W. Herrebout, J. G. Knight and M. J. Hall, *Chem. Eur. J.*, 2016, **22**, 93–96.
5. Z. Wang, A. A. Sukhanov, A. Toffoletti, F. Sadiq, J. Zhao, A. Barbon, V. K. Voronkova and B. Dick, *J. Phys. Chem. C*, 2019, **123**, 265–274.